Environ Monit Assess (2019) 191: 194
https://doi.org/10.1007/s10661-019-7343-1

# Spatial variability of urban climate in response to quantitative trait of land cover based on GWR model

**Xisheng Hu · Hanqiu Xu**

Received: 13 October 2018 / Accepted: 19 February 2019 / Published online: 27 February 2019


**Abstract** Land surface temperature and moisture are central components of the Earth's surface heat budget. China has experienced substantial land use/cover change that has led to deterioration of the urban microclimate, thus affecting global climate change. Understanding the spatial non-stationarity in the relationships between climate and land cover across a highly heterogeneous surface of urban landscapes is important for improving urban planning and management. This study used Landsat-8 OLI/TIRS data to explore the relationship of the three components (index-based built-up index (IBI); bare soil index (SI); and normalized difference vegetation index (NDVI)) with the urban climate (land surface temperature (LST) and land surface moisture (LSM)) using both a global model (ordinary least squares (OLS)) and a local model (geographically weighted regression (GWR)) for a megacity in Southeast China. The global regression results showed that there were significant positive correlations between the LST and the IBI and SI, while significant negative correlations were observed between the LST and the NDVI; opposite results were observed for the LSM. The IBI is the factor having the greatest impact on the LST, while the SI is among the most important factors for the LSM. The local regression results showed that the response of urban climate to land surface is affected greatly by water areas, but the role of the water areas is impacted by their size and surrounding landscape patterns. Moreover, the effects of vegetation and built-up land on the urban climate vary across locations with different wind patterns.

**Keywords** Global climate change · Geographically weighted regression · Land surface temperature · Land surface moisture · Land use/cover change · Fuzhou

X. Hu · H. Xu (✉)
College of Environment and Resources, Fuzhou University, Fuzhou 350108 Fujian, China
e-mail: hxu@fzu.edu.cn

X. Hu
College of Transportation and Civil Engineering, Fujian Agriculture and Forestry University, Fuzhou 350002 Fujian, China

H. Xu
Institute of Remote Sensing Information Engineering, Fuzhou University, Fuzhou 350108 Fujian, China

H. Xu
Fujian Provincial Key Laboratory of Remote Sensing of Soil Erosion and Disaster Protection, Fuzhou, China

## Introduction

Land use/cover change (LUCC) is one of the main driving forces for global climate change and has become a global environmental issue (Stocker et al. 2013; Hereher 2017), particularly in developing countries (Li et al. 2009). Though climate change may be a global phenomenon, its effects are borne out at local scales worldwide (Dickinson et al. 2017). At local scales, microclimate patterns are shaped by physical characteristics, such as the properties of underlying surfaces (Pielke et al. 2011). This phenomenon and the

underlying mechanisms have been well documented in the urban heat island (UHI) literature (Lowry 1977; Oke 1982; Stewart 2000), where cities have been found to be warmer than their surrounding areas. In this context, a growing body of research has focused on predicting and analyzing the local impacts of LUCC on climate change (Barros et al. 2014). Previous studies typically use time series analysis at selected locations experiencing LUCC, comparing the climate change (e.g., land surface temperature (LST)) for each location before and after the change (Hereher 2017). Although LUCC may significantly affect local climate, the magnitude of its effects is controversial. Little is known about how this relationship is affected by high landscape heterogeneity. The impacts of LUCC on local climate are poorly understood and warrant further study.

LST is a common proxy for representing the heat budget of the Earth's surface and the trends of climate change at different spatial scales (Srivastava et al. 2009; Amiri et al. 2009; CWT et al. 2014). Hence, LST has been employed as an indicator in numerous studies to understand the complex processes of land surface change, such as drought monitoring (Cai et al. 2017); greenhouse effects (Nes et al. 2015); hydrological simulation (Mo and Lettenmaier 2014); urban heat island analysis (Weng 2009; Rajasekar and Weng 2009; Pichierri et al. 2012); epidemiological modeling (Goetz et al. 2000); and snowpack investigation (Shamir and Georgakakos 2014). Another measurement metric, soil moisture, plays a key role not only in heat budgets but also in hydrological processes at the Earth's surface (Kerr et al. 2001; Zhuo et al. 2015). Specifically, land surface moisture (LSM) has been widely recognized as an essential measure in many environmental studies. For example, Wanders et al. (2014) found that the parameters related to land surface processes can be identified accurately when incorporating satellite-retrieved LSM into large-scale hydrological models (Wanders et al. 2014). In this context, LST and LSM were employed in this study as indicators of the urban climate.

Previous studies have revealed that the features of LUCC can be identified by applying the normalized difference vegetation index (NDVI) (Hereher 2017); this index has been regarded as the most commonly used spectral transform (Fung and Siu 2000; Muttitanon and Tripathi 2005; Sahebjalal and Dashtekian 2013) and has been applied extensively to observe LUCC in many cases (Fuller 1998; Waylen et al. 2014; Eckert et al. 2015; Nguyen et al. 2015). It is well known that the effect of vegetation on the reduction of LST is clearly due to the process of evapotranspiration (Yuan and Bauer 2007). On the other hand, the LUCC from vegetation to built-up areas has a great impact on the energy budget by altering the permeability of the land surface, leading to an increase in LST (Guo et al. 2012). In general, the features of the underlying surface in a region have a great impact on the distribution of water and heat, thus determining the climate. Quantifying the relationship between vegetation (NDVI) and temperature (LST) has attracted much research attention (Weng et al. 2004; Xu et al. 2009). Most of these studies are based on global regression models, and understanding of the spatial variations in the associations between vegetation and climate is still insufficient; moreover, the other key components of the urban ecosystem, the built-up area and the bare surface area associations with urban climate, have not been quantitatively analyzed in detail due to the lack of a suitable index (Xu et al. 2009). Recently, Xu et al. (2009) proposed a thematic-oriented index (index-based built-up index (IBI)) to delineate built-up areas based on the three commonly used indices, including the soil-adjusted vegetation index (SAVI); the modified normalized difference water index (MNDWI) (Xu 2006); and the normalized difference built-up index (NDBI) (Zha et al. 2003). The IBI can enhance the built-up land features effectively because the subtraction of the SAVI and MNDWI bands from the NDBI band produces positive values for built-up area pixels only. In addition to built-up areas, a bare soil index (SI) was employed to delineate patches of bare land or sparsely vegetated land occurring in deforested areas or in abandoned locations across the study area (Hu and Xu 2018). Thus, NDVI, IBI, and SI were all selected here to represent land surface features in this study.

Fuzhou city is located in the estuary lowland area of the Minjiang River in Fujian province of southeastern China, which has experienced very rapid economic development over the past three decades. Its GDP ranks 29th in the top 100 of China's cities in 2016 (http://gov.finance.sina.com.cn). With economic development, the built-up area of the city has changed rapidly from very small, isolated population centers to large, interconnected urban centers over the past three decades, and this city has experienced continuous warming during the past decade, becoming a new "stove" in China. Therefore, this region presents a particularly interesting

laboratory for studying spatial patterns of urban climate and land cover. The spatial distribution of the climate factors (LST and LSM) varies depending on the land cover type (Voogt and Oke 2003; Ali and Shalaby 2012 ). However, the challenge of capturing the high spatial heterogeneity in urban areas exists when employing global regression models. To overcome the limitations of previous studies, which are discontinuous in space by comparing the microclimate change intra- or inter-locations, we employed a local regression model (geographically weighted regression (GWR)) to explore the spatial non-stationarity in the relationships between climate (LST, LSM) and land cover (NDVI, ISI, and SI) across a continuous land surface in urban landscapes of high heterogeneity; then, we identified areas with strong coupling of vegetation to climate anomalies. This study can serve as another example of using remote sensing to study the LUCC under an urban climate and provide a scientific basis for urban planning to mitigate urban climate change.

## Methods and materials

### Study area

Fuzhou city is the capital and the largest prefecture-level city in Fujian province, China, located in southeast China. There were 7.66 million residents in 2017 in the city, with a per capita GDP of US $15,000 in 2017. It ranked 25th in China's Top 100 Cities in 2017. It has been observed that the temperature has continued to rise during the past 20 years (Hu et al. 2015; Cai et al. 2017). Consequently, exploration of the spatial variations in the urban climate associated with land surface is essential. More information on the study area can be found in the reference (Hu and Xu 2018).

### Data resources and preprocessing

The Landsat OLI/TIRS images (30 × 30 m) employed in this study were acquired on 2016-06-25, when less cloud cover was present. The preprocessing of the images included radiation calibration and atmospheric correction, based on the guide for Landsat-8 algorithm (http://glovis.usgs.gov/CDR_LSR.php). The digit numbers (DNs) of the images were converted into reflectance values of the planetary surface (Xu et al. 2013; Kilic et al. 2016).

### Retrieval of land cover and urban climate indices

In terms of the LUCC, the most prominent feature is the change from ecological lands to built-up lands or bare lands (Foley et al. 2005; Sun et al. 2010; Seddon et al. 2016). Thus, IBI and SI were applied to represent the built-up lands and bare lands, respectively, and NDVI was selected as an indicator of ecological lands. As discussed in our introduction, LST and LSM were utilized to represent local climate agencies. Additionally, clouds and their shadows were masked based on very low temperatures (Malbéteau et al. 2017); water patches were also masked based on the MNDWI, using the method of manual debugging threshold value (Xu 2006). The detailed calculation formulae for IBI, SI, NDVI, LST, LSM, and MNDWI can be obtained from our previously published literature (Xu 2006; Hu and Xu 2018) and will not be described in detail here.

### Regression models

Both a global model (ordinary least squares (OLS)) and a local model (GWR) were employed to examine the association between urban climate (LST and LSM) and land surface features (IBI, SI, and NDVI). OLS assumes that the relationship between dependent and independent variables is consistent within the entire study region, while GWR recognizes the spatial heterogeneity in the interaction between the two regressors across locations (Zawadzki et al. 2005; Fotheringham et al. 2016). Much research has proven that the GWR model is more effective than the OLS model (Hu et al. 2015). The detailed formulae of the two regression models are specified in the references (Poudyal et al. 2012; Hu et al. 2015; Fotheringham et al. 2016).

For our case, both the OLS and GWR models were estimated using the ArcGIS 10.0 program. For GWR models, the Gaussian equation was adopted, using a fixed distance according to the Akaike information criterion (AIC). The goodness of fit of the GWR model was tested using a set of parameters, including the adjusted $R$-squared; $P$ value; residual squares; Moran's $I$; and AIC: (1) The value of the adjusted $R$-squared is between 0 and 1, with a higher value representing better simulation results. (2) The $P$ value is widely used in statistical hypothesis testing, with a threshold value of

5%. (3) The residual squares are the sum of the squares of residuals (deviations predicted from actual empirical values of data). A small residual square indicates a tight fit of the model to the data. (4) Moran's *I* was used to evaluate if the regression residuals are randomly distributed in space. A small Moran's *I* value indicates a random distribution of the residual squares, indicating the goodness of fit of the GWR model. (5) The AIC is a relative estimator of the goodness of fit of a statistical model. If the difference between the AIC values of the two models exceeds three, a model with a lower AIC value is considered to be the better one.

### Variables

Variations of urban climate in response to changes in land cover were observed, using urban climate (LST and LSM) as dependent variables, and the land surface features (IBI, SI, and NDVI) as independent variables. In our analysis, six separate models were defined, with one dependent variable and one independent variable being involved in each model to eliminate multicollinearity problems. The variables are described in Table 1.

## Results

### Description of the regression outcomes

Table 2 indicates the regression results of the OLS and GWR models for the association between urban climate and land features. The adjusted $R^2$ values of the GWR models ranged from 0.784 to 0.959, higher than those of the OLS models (0.002–0.832). The AIC and the residual squares of the GWR models were all smaller than those for the OLS models, except for the residual squares in the model of LSM and IBI. Moreover, the values of Moran's *I* were relatively small, ranging from 0.021 to 0.125; Figs. 2, 3, 4, 5, and 6 (right) also revealed that the residuals of each model were randomly distributed across the study area. Based on the above results, we conclude that the fitting effect of the GWR models was better than the OLS results. All six GWR models were statistically significant at the 0.1% level, which also indicated a high goodness of fit for the locally weighted regression models.

Table 3 presents a summary of coefficients of the GWR and the OLS models. In Table 3, the values of minimum, average, median, maximum, and standard deviation are listed. These statistics enabled a comparison of the coefficient values of each independent variable and revealed how greatly the coefficients varied across the study region. In summary, the impacts on the LST (from large to small) were in the order of IBI, SI and NDVI, while the impacts on the LSM (from large to small) were in the order of SI, NDVI, and IBI; moreover, both positive and negative effects coexisted in all cases.

### Spatial variations in the response of LST to land cover

Grid-level regression coefficients estimated by GWR were mapped in Figs. 1, 2, 3, 4, 5, and 6 (left). In these maps, the natural break classification method (Jenks) was used to divide the coefficients into five categories, with zero being artificially set as a demarcation point to distinguish the positive and negative correlations for all maps in terms of the GWR coefficients.

Figure 1 shows that the positive relationships between the LST and the IBI are distributed across most of the study area, while there are very few portions of the grids with negative associations randomly distributed in the study area. This indicated that the LST increased gradually with an increase in the IBI, whereas the rates of increase varied significantly across the region. The positive correlation coefficients were extensively and noticeably higher along the north border and in some relatively smaller clusters (e.g., the central cluster, the southeast corner cluster, and the southwest cluster) compared to those in other regions. A large green cluster, located close to the river and including the inland river, exhibited a lower level of positive correlation.

Figure 2 also indicates that the positive relationships between the LST and the SI are distributed across most of the study area and displayed clustering similar to that seen in Fig. 1. Compared to Fig. 1, an obvious feature in Fig. 2 was the narrow stripes close to the river, indicating clearly negative associations between the LST and the SI; the negative correlation was more pronounced in areas closer to the river. This negative relationship transitioned to positive values at a distance of approximately 1 to 2 km from the river.

Figure 3 reveals the spatial variations in the relationships between the LST and the NDVI. There were narrow stripes closer to the river, indicating noticeably positive associations between

**Table 1** Description of the dependent and independent variables used in the regression models

| Variables | | Minimum | Average | Maximum | Standard deviation |
|---|---|---|---|---|---|
| Dependent | LST | 26.685 | 39.133 | 52.403 | 4.726 |
| | WET | − 0.369 | − 0.100 | 0.094 | 0.066 |
| Independent | IBI | − 0.656 | − 0.150 | 0.095 | 0.143 |
| | SI | − 0.378 | − 0.068 | 0.160 | 0.114 |
| | NDVI | − 0.519 | 0.396 | 0.886 | 0.305 |

the LST and the NDVI; the positive correlation is greater in areas closer to the river. This was in contrast to the correlation between the LST and the SI. The width of the belt showing positive values for the relationship between the LST and the NDVI was greater (approximately 2 to 3 km) than the width of the belt showing negative values for the relationship between the LST and the SI.

## Spatial variations in the response of the LSM to land cover

Figure 4 demonstrates that the relationship between the LSM and the IBI was negative for most of the study area, while there were also a few clusters indicating positive associations scattered across the study area. This indicated that the LSM decreased as the IBI increased in most locations, but that there were still some areas showing a synergistic relationship between the LSM and the IBI. This figure also shows that the areas of negative correlations along the river zone, including the inland rivers and the reservoirs, were larger than for the inland locations.

Figure 5 also indicated that the negative relationships between the LSM and the SI were distributed across most of the study area, but that there were narrow stripes close to the river, indicating strongly positive associations between the LSM and the SI; most of the areas with positive correlations tended to be distributed near the rivers. For the areas showing negative correlations between the LSM and the SI, their magnitude was greater in the areas near inland rivers or reservoirs than those in other areas.

Figure 6 reveals the spatial variations in the relationships between the WET and the NDVI, demonstrating that there were narrow stripes close to the river, indicating noticeably negative associations between the LSM and the NDVI; the negative correlations were more pronounced with decreasing distances from the river, while there were positive correlations in other areas. This result was in contrast to the correlation between the LSM and the SI; moreover, the belt width of positive

**Table 2** Comparison of results between OLS (global model) and GWR (local model)

| Dependent variables | Independent variables | GWR | | | | | OLS | | | |
|---|---|---|---|---|---|---|---|---|---|---|
| | | Adjusted *R*-squared | AIC | Residual squares | *P* value | Moran's *I* | Adjusted *R*-squared | AIC | Residual squares | *P* value |
| LST | IBI | 0.959 | 21,990.865 | 6225.837 | 0.001 | 0.025 | 0.832 | 32,443.428 | 29,268.500 | 0.001 |
| | SI | 0.886 | 29,979.713 | 16,558.415 | 0.001 | 0.040 | 0.040 | 46,025.045 | 167,108.000 | 0.001 |
| | NDVI | 0.832 | 32,586.880 | 27,916.078 | 0.001 | 0.125 | 0.073 | 45,754.880 | 161,416.000 | 0.05 |
| LSM | IBI | 0.784 | − 31,820.328 | 6.228 | 0.001 | 0.021 | 0.875 | − 36,569.278 | 4.189 | 0.001 |
| | SI | 0.813 | − 32,805.093 | 5.626 | 0.001 | 0.024 | 0.002 | − 20,365.115 | 33.464 | 0.001 |
| | NDVI | 0.786 | − 32,231.092 | 6.839 | 0.001 | 0.072 | 0.277 | − 22,879.420 | 24.239 | 0.001 |

**Table 3** Parameter descriptive statistics from the OLS (global model) and GWR (local model)

| Dependent variables | Independent variables | OLS | GWR | | | | |
|---|---|---|---|---|---|---|---|
| | | | Minimum | Average | Median | Maximum | Standard deviation |
| LST | IBI | 27.959 | − 2.767 | 29.492 | 28.679 | 55.395 | 7.892 |
| | SI | 9.487 | − 131.223 | 6.394 | 19.589 | 49.277 | 31.928 |
| | NDVI | − 1.749 | − 26.116 | − 2.441 | − 1.061 | 16.793 | 13.119 |
| WET | IBI | − 0.194 | − 1.377 | − 0.378 | − 0.379 | 0.562 | 0.303 |
| | SI | − 0.477 | − 1.123 | − 0.036 | − 0.263 | 2.599 | 0.531 |
| | NDVI | 0.228 | − 0.275 | − 0.021 | − 0.034 | 0.384 | 0.170 |

correlations in the relationship between the LSM and the NDVI was larger than that for the negative correlations seen in the relationship between the LSM and the SI, which was approximately 2 to 3 km from the river.

## Discussions

### Urban climate and land surface

The OLS regression outcomes indicated a significant positive correlation between IBI, SI, and LST, while a significantly negative correlation was seen between NDVI and LST; contrasting results were obtained in terms of the LSM. This is in accordance with the findings related to the urban heat island (UHI) effect in Quanzhou city, in the same Chinese province (Xu et al. 2009), and in the megacities of Southeast Asia (Estoque et al. 2017). These previous studies indicated that there was a significant positive correlation between mean LST and the density of impervious surfaces, while this correlation was negative for green space. This is because built-up lands promote sensible heat exchange, leading to an aggravation of the UHI effect, while greater vegetation coverage leads to higher rates of evapotranspiration, promoting latent heat exchange for reduction of LST (Wilson et al. 2003).

We also found that the coefficient values of the IBI were greater than that of the NDVI (Table 3). Our results of the correlations are consistent with earlier findings, indicating that impervious surfaces have a higher impact

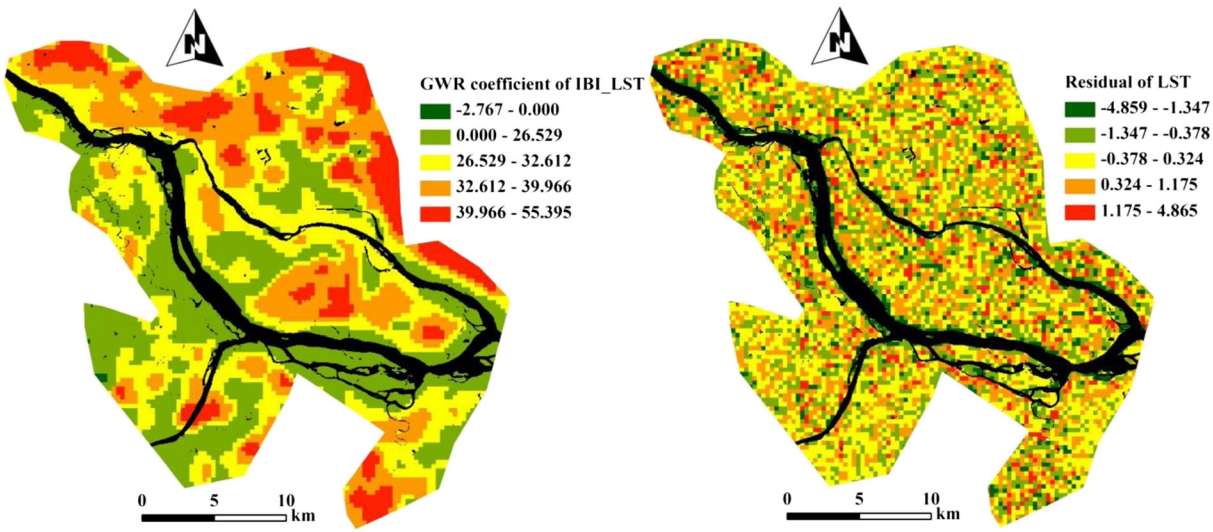


**Fig. 1** GWR coefficient (left), residual of IBI (right) against LST; the black background shows water areas; this convention is maintained for subsequent figures

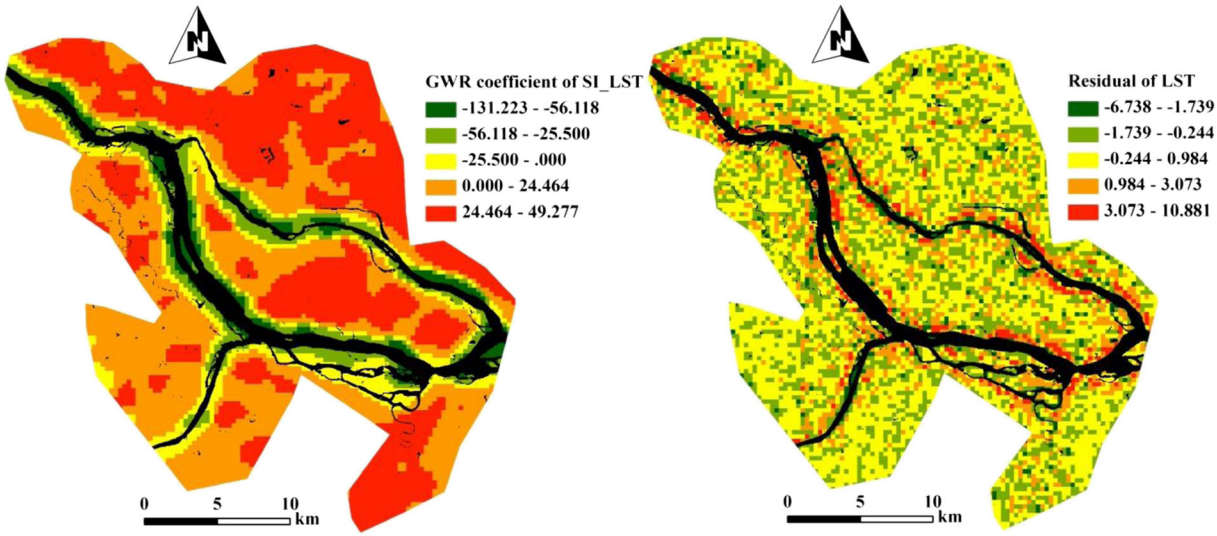


**Fig. 2** GWR coefficient (left), residual of SI (right) against LST

on LST than green space (Ma et al. 2016; Estoque et al. 2017). Estoque et al. (2017) indicated that the beta value of impervious surfaces vs. LST was higher than that for green space vs. LST; Xu et al. (2009) suggested that the IBI can explain 91.2 to 94.5% of the LST variation in urban areas. Expanding from previous studies, we also explored the relationship between the LSM and land cover, which indicated that the SI has a higher impact on LSM than the IBI and NDVI. This is mainly because the SI, including the combination information of bare soil surface; built-up land; and sand surfaces (Rikimaru et al. 2002), are dry areas but are not necessary at high temperatures, because a large part of the soil areas is under/near trees or near rivers (beaches).

It has been recognized that the effects of the land cover on the LST and the LSM may differ greatly across study areas (Zhou et al. 2016), which can be due to the different spatial combinations of impervious surfaces; green space; and underlying bio-geophysical factors (Winckler et al. 2017; Estoque et al. 2017). In this context, the global regression model (OLS) assumes that the relationship between the dependent variables and independent variables is constant across the study area (i.e., the values of β0 and β1 are the same for every

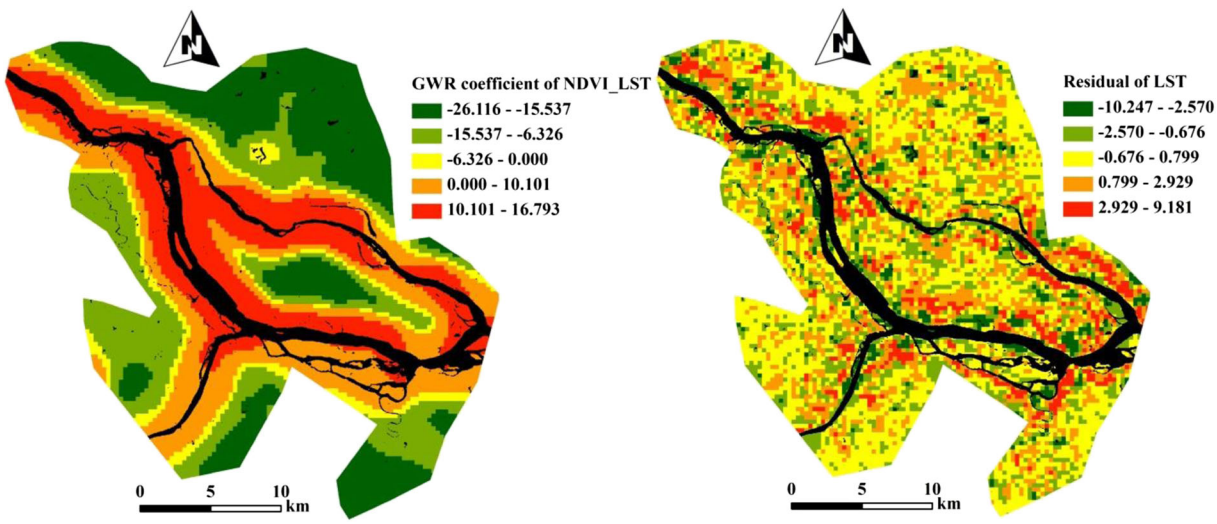


**Fig. 3** GWR coefficient (left), residual of NDVI (right) against LST

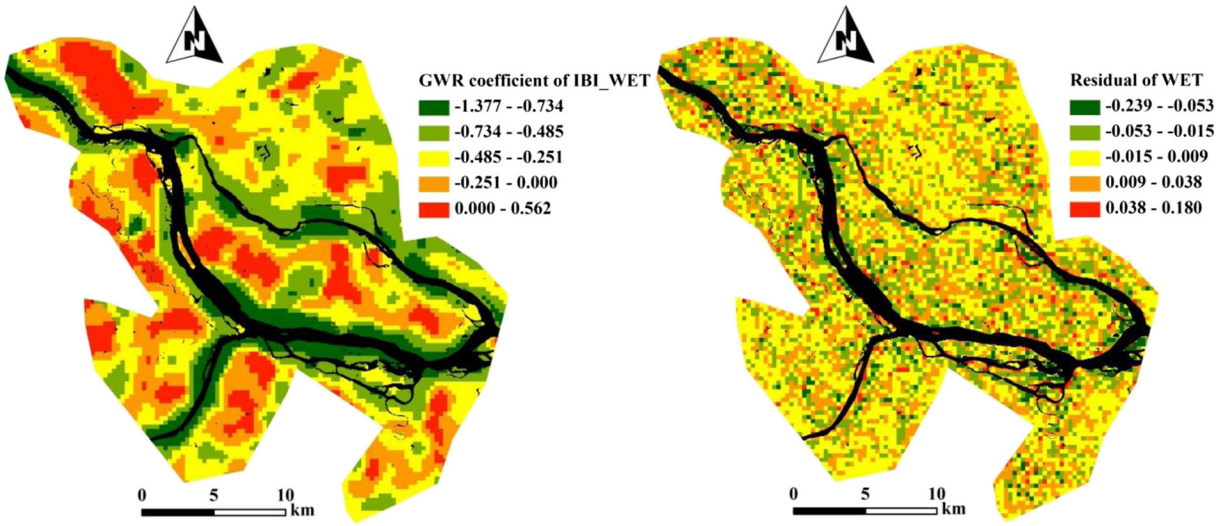


**Fig. 4** GWR coefficient (left), residual of IBI (right) against LSM

possible location in the study area) and may lead to bias when spatial variations in the relationship between the urban climate and the land cover exist. Therefore, this study further explored the relationship using GWR models, which is a powerful tool for exploring spatial heterogeneity (Fotheringham et al. 2016).

## Spatial variations in the associations of urban climate and land surface

We found that heterogeneity of the land-cover mosaic inside the urban area entails the complexity in the spatial distributions of LST and LSM. The relationships between urban climate and urban surfaces have been well established and were discussed in a previous section of this paper. However, the spatial variations in the relationships have been less thoroughly explored. Our results confirm that the GWR provides a considerable improvement over the OLS regressions. Though the general spatial pattern of LST and LSM predicted by the OLS and the GWR models seems similar (Table 3), the GWR is able to highlight areas that are locally hot or dry (Figs. 1, 2, 3, 4, 5, and 6), but the OLS cannot depict such areas. Figs. 1, 2, 3, 4, 5, and 6 indicate the spatial variations in the GWR regression coefficients and the residual across locations, revealing the high

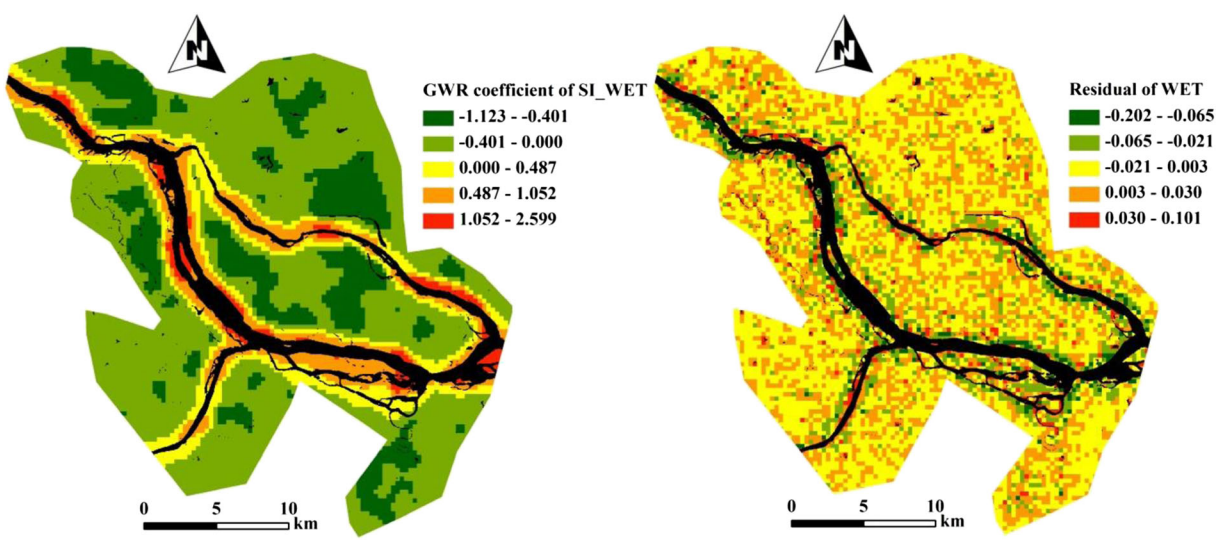


**Fig. 5** GWR coefficient (left), residual of SI (right) against LSM

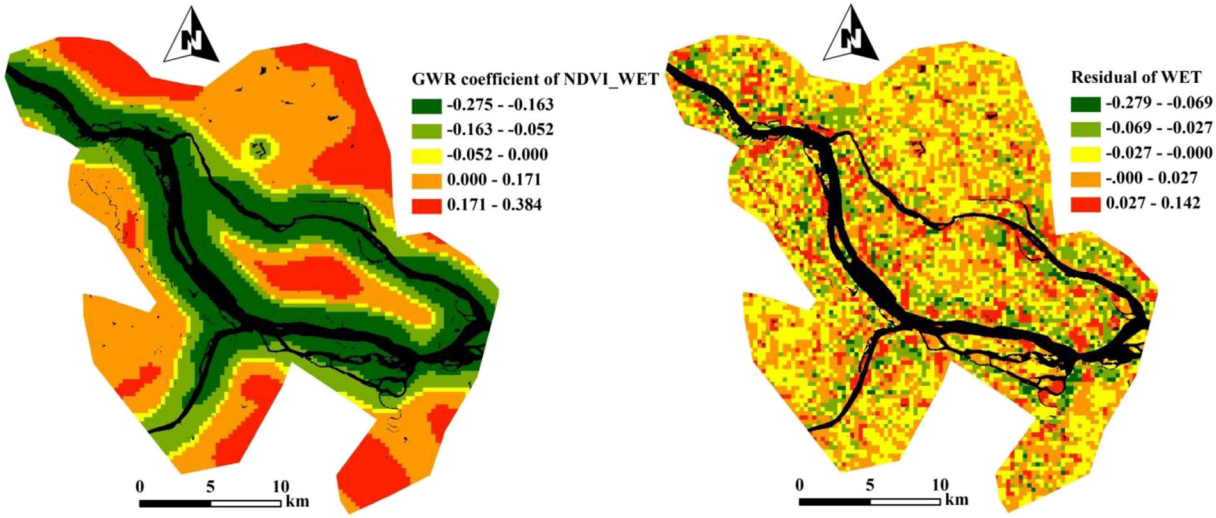


**Fig. 6** GWR coefficient (left), residual of NDVI (right) against LSM

heterogeneity in the relationship between climate and land surfaces in urban area.

The distribution of the local coefficients of GWR has several obvious features:

1) The response of urban climate to land surface is affected greatly by water areas, whether a large regional river (Minjiang River) or urban inland rivers. In some cases, the rivers can mitigate the negative effect of the built-up land on the LST and the bare land on the LSM, e.g., the clusters closer to the river exhibited a lower level of negative impact of the built-up land on the LST (Fig. 1); the relationship between the LSM and the SI becomes positive on the near the rivers (Fig. 5); in some cases, the positive effect of vegetation cover on both the LST and the LSM is eliminated; it is unexpected that a positive correlation between the LST and the NDVI was observed on both sides of the rivers (Fig. 3), and it is also interesting that a negative association between the LSM and the NDVI was identified on the riverbanks (Fig. 6); in another case, the rivers may exacerbated the negative effect of the bare land on the LST and the built-up land on the LSM, e.g., greater negative correlation between the LST and the SI was found in the both sides of the rivers, and areas closer to rivers showed greater negative correlations (Fig. 2); this is the same association between the LSM and the IBI (Fig. 4).
2) The role of water areas is affected by their size and surrounding land cover. Using the relationship between the LST and the NDVI as one case (Fig. 3), the association was strongly positive on both sides of the wide rivers, while there was a slight negative

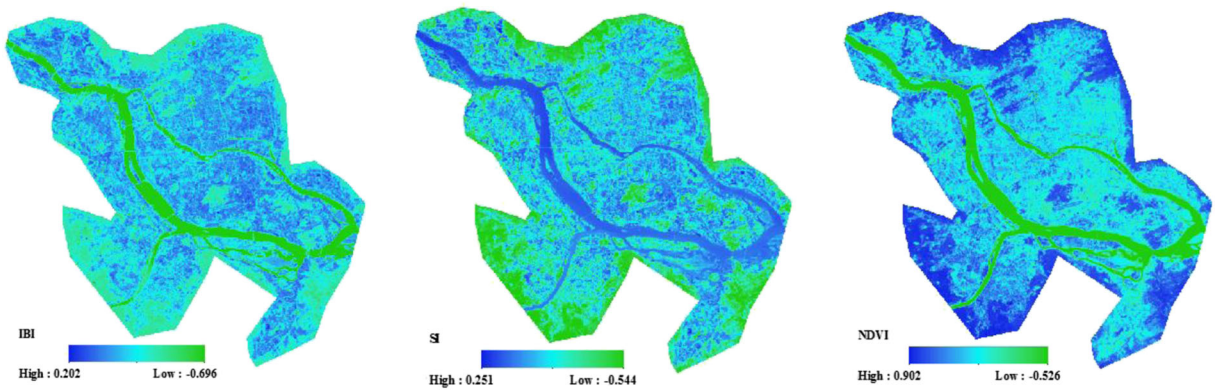


**Fig. 7** Distribution of IBI, SI, and NDVI

association for areas surrounding the lake with a higher negative relation on the both sides of the narrow rivers. It is worth noting that there were still extremely negative effects of the NDVI on the LST in the vicinity of the lakes in the northern part of the study area. This is because the areas surrounding the lakes in the northern part are forested, while the areas around the lakes are mostly built-up land. This shows the combined effects of vegetation, buildings, and other characteristics of urban surfaces. Our results are in agreement with a previous study (Buyantuyev and Wu 2010), which verified the combined effects of vegetation and built-up lands for explaining spatio-temporal variation of temperatures in Phoenix.

3) The positive (NDVI) and negative (IBI and SI) effects are greater in areas with low wind levels. The dominant wind direction in the study area during the study period (summer) is SE and the study region is surrounded by mountains. Therefore, the magnitude of the coefficients of LST vs. NDVI and LSM vs. NDVI was greater in the north-western part of the mountains in the study area (Figs. 3 and 6). Moreover, the negative effects of built-up land on the LST (bare land on both the LST and the LSM) were also greater in north-western part of the mountain and the study area (Figs. 1 and 2). The exception was the relationship between the IBI and the LSM (Fig. 4). In addition to the higher negative correlation at near rivers, the lower outlet area still had a higher negative correlation than the upper outlet area. Some clusters (red areas in Fig. 4) showed positive correlation between the IBI and LSM. This is mainly because these areas have high-density buildings (Fig. 7) with lower direct sunlight levels and therefore are damper.

## Conclusions

This study used Landsat-8 OLI/TIRS data to explore the relationship of the three components (IBI, SI, and NDVI) with the urban climate (LST and LSM) by use of both OLS and GWR regressions in the megacities of Southeast China. The OLS regression outcomes indicated a significant positive correlation between IBI, SI, and LST, while a significant negative correlation between NDVI and LST was observed; opposite results were obtained in terms of the LSM. We also found that the impact of the IBI on the LST was greater than that of the NDVI and the SI, while the impact of the SI on the LSM was greater than that of the other two indicators.

The spatial patterns of GWR coefficients indicated that (1) the response of urban climate to land surface is affected greatly by areas of water, whether a large regional river (Minjiang River) or urban inland rivers. Rivers may reduce the positive effects of vegetation on the LST and LSM, mitigate the negative effect of the built-up land on the LST and the bare land on the LSM, and exacerbate the negative effect of the bare land on the LST and the built-up land on the LSM. (2) The role of water areas is affected by their size and the combined effects of surrounding lands. Large river areas may offset the cooling effect of vegetation, while small rivers may reduce the cooling effect of vegetation. (3) The effect on the urban climate is affected by the prevalence of winds. Vegetation has a greater positive effect in areas with less wind, while the negative effects of buildings in places with poor wind circulation are exacerbated.

**Funding information** This research was funded by the China Postdoctoral Science Foundation (no. 2017M610390), the National Natural Science Foundation of China (no. 41201100), and the Natural Science Foundation of Fujian Province (no. 2015J01606), to which we are very grateful.

**Compliance with ethical standards**

**Conflict of interest** The authors declare that there is no conflict of interest.



## References

Ali, R. R., & Shalaby, A. (2012). Response of topsoil features to the seasonal changes of land surface temperature in the arid environment. *International Journal of Soil Science, 7*, 39–50.

Amiri, R., Weng, O., Alimohammadi, A., & Alavipanah, A. (2009). Spatial-temporal dynamics of land surface temperature in relation to fractional vegetation cover and land use/cover in the Tabriz urban area, Iran. *Remote Sensing of Environment, 113*, 2606–2617.

Barros, V. R., Field, C. B., Dokken, D. J., Mastrandrea, M. D., Mach, K. J., Bilir, T. E., Chatterjee, M., Ebi, K. L., Estrada, Y.

O., Genova, R. C., Girma, B., Kissel, E. S., Levy, A. N., MacCracken, S., Mastrandrea, P. R., & White, L. L. (eds). (2014). IPCC, 2014: climate change 2014: impacts, adaptation, and vulnerability. Part B: regional aspects. Contribution of working group II to the fifth assessment report of the intergovernmental panel on climate change. Cambridge: Cambridge University Press.

Buyantuyev, A., & Wu, J. (2010). Urban heat islands and landscape heterogeneity: linking spatiotemporal variations in surface temperatures to land-cover and socioeconomic patterns. *Landscape Ecology, 25*, 17–33.

Cai, Y. L., Chen, G., Wang, Y. L., & Yang, L. (2017). Impacts of land cover and seasonal variation on maximum air temperature estimation using MODIS imagery. *Remote Sensing, 9*, 233.

Core Writing Team (CWT), Pachauri, R. K., & Meyer, L. A. (2014). *Climate change 2014. Synthesis report. Contribution of Working Groups I, II and III to the Fifth Assessment Report of the Intergovernmental Panel on Climate Change*. Geneva: Intergovernmental Panel on Climate Change (IPCC).

Dickinson, K. L., Monaghan, A. J., Rivera, I. J., Hu, L., Kanyomse, E., Alirigia, R., Adoctor, J., Kaspar, R. E., Oduro, A. R., & Wiedinmyer, C. (2017). Changing weather and climate in northern Ghana: comparison of local perceptions with meteorological and land cover data. *Regional Environmental Change, 17*(3), 915–928.

Eckert, S., Hüsler, F., Liniger, H., & Hodel, E. (2015). Trend analysis of MODIS NDVI time series for detecting land degradation and regeneration in Mongolia. *Journal of Arid Environments, 113*, 16–28.

Estoque, R. C., Murayama, Y., & Myint, S. W. (2017). Effects of landscape composition and pattern on land surface temperature: an urban heat island study in the megacities of Southeast Asia. *Science of the Total Environment, 577*, 349–359.

Foley, J. A., De Fries, R., Asner, G. P., Barford, C., Bonan, G., Carpenter, S. R., Chapin, F. S., Coe, M. T., Daily, G. C., Gibbs, H. K., Helkowski, J. H., Holloway, T., Howard, E. A., Kucharik, C. J., Monfreda, C., Patz, J. A., Prentice, I. C., Ramankutty, N., & Snyder, P. K. (2005). Global consequences of land use. *Science, 309*, 570–574.

Fotheringham, A. S., Charlton, M. E., & Brunsdon, C. (2016). Geographically weighted regression: a natural evolution of the expansion method for spatial data analysis. *Environment and Planning A, 30*, 1905–1927.

Fuller, D. O. (1998). Trends in NDVI time series and their relation to rangeland and crop production in Senegal, 1987–1993. *International Journal of Remote Sensing, 19*, 2013–2018.

Fung, T., & Siu, W. (2000). Environmental quality and its changes, an analysis using NDVI. *International Journal of Remote Sensing, 21*, 1011–1024.

Goetz, S. J., Prince, S. D., & Small, J. (2000). Advances in satellite remote sensing of environmental variables for epidemiological applications. *Advances in Parasitology, 47*, 289–307.

Guo, Z., Wang, S. D., Cheng, M. M., & Shu, Y. (2012). Assess the effect of different degrees of urbanization on land surface temperature using remote sensing images. *Procedia Environmental Sciences, 13*, 935–942.

Hereher, M. E. (2017). Effect of land use/cover change on land surface temperatures—the Nile Delta, Egypt. *Journal of African Earth Sciences, 126*, 75–83.

Hu, X. S., & Xu, H. (2018). A new remote sensing index for assessing the spatial heterogeneity in urban ecological quality: a case from Fuzhou City, China. *Ecological Indicators, 89*, 11–21.

Hu, X. S., Hong, W., Qiu, R. Z., Hong, T., Chen, C., & Wu, C. Z. (2015). Geographic variations of ecosystem service intensity in Fuzhou city, China. *Science of the Total Environment, 512*, 215–226.

Kerr, Y. H., Waldteufel, P., Wigneron, J. P., Martinuzzi, J., Font, J., & Berger, M. (2001). Soil moisture retrieval from space: the soil moisture and ocean salinity (SMOS) mission. *IEEE Transactions on Geoscience and Remote Sensing, 39*(8), 1729–1735.

Kilic, A., Allen, R., Trezza, R., Ratcliffe, I., Kamble, B., Robison, C., & Ozturk, D. (2016). Sensitivity of evapotranspiration retrievals from the METRIC processing algorithm to improved radiometric resolution of Landsat 8 thermal data and to calibration bias in Landsat 7 and 8 surface temperature. *Remote Sensing of Environment, 185*, 198–209.

Li, J., Wang, X., Wang, X., Ma, M., & Zhang, H. (2009). Remote sensing evaluation of urban heat island and its spatial pattern of the Shanghai metropolitan area, China. *Ecological Complexity, 6*, 413–420.

Lowry, W. P. (1977). Empirical estimation of the urban effects on climate: a problem analysis. *Journal of Applied Meteorology, 16*, 129–135.

Ma, Q., Wu, J., & He, C. (2016). A hierarchical analysis of the relationship between urban impervious surfaces and land surface temperatures: spatial scale dependence, temporal variations, and bioclimatic modulation. *Landscape Ecology, 31*, 1139–1153.

Malbéteau, Y., Merlin, O., Gascoin, S., Gastellu, J. P., Mattar, C., Olivera-Guerra, L., Khabba, S., & Jarlan, L. (2017). Normalizing land surface temperature data for elevation and illumination effects in mountainous areas: a case study using aster data over a steep-sided valley in Morocco. *Remote Sensing of Environment, 189*, 25–39.

Mo, M. C., & Lettenmaier, D. P. (2014). Hydrologic prediction over the conterminous United States using the national multimodel ensemble. *Journal of Hydrometeorology, 15*, 1457–1472.

Muttitanon, W., & Tripathi, N. (2005). Land use/land cover changes in the coastal zone of Ban Don Bay, Thailand using Landsat 5 TM data. *International Journal of Remote Sensing, 26*, 2311–2323.

Nes, E. H. V., Scheffer, M., Brovkin, V., Lenton, T. M., Ye, H., Deyle, E., & Sugihara, G. (2015). Causal feedbacks in climate change. *Nature Climate Change, 5*, 445–448.

Nguyen, O. V., Kawamura, K., Trong, D., Gong, Z., & Suwandana, E. (2015). Temporal change and its spatial variety on land surface temperature and land use changes in the Red River Delta, Vietnam, using MODIS time-series imagery. *Environmental Monitoring and Assessment, 187*, 1–11.

Oke, T. R. (1982). The energetic basis of the urban heat island. *Quarterly Journal of the Royal Meteorological Society, 108*, 1–24.

Pichierri, M., Bonafoni, S., & Biondi, R. (2012). Satellite air temperature estimation for monitoring the canopy layer heat island of Milan. *Remote Sensing of Environment, 127*, 130–138.

Pielke, R. A., Pitman, A., Niyogi, D., Mahmood, R., McAlpine, C., Hossain, F., Goldewijk, K. K., Nair, U., Betts, R., Fall, S., Reichstein, M., Kabat, P., & Noblet, N. (2011). Land use/land cover changes and climate: modeling analysis and observational evidence. *WIREs Climate Change, 2*, 828–850.

Poudyal, N. C., Johnson-Gaither, C., Goodrick, S., Bowker, J. M., & Gan, J. B. (2012). Locating spatial variation in the association between wildland fire risk and social vulnerability across six southern states. *Environmental Management, 49*, 623–635.

Rajasekar, U., & Weng, Q. (2009). Urban heat island monitoring and analysis using a non-parametric model: a case study of Indianapolis. *ISPRS Journal of Photogrammetry and Remote Sensing, 64*, 86–96.

Rikimaru, A., Roy, P. S., & Miyatake, S. (2002). Tropical forest cover density mapping. *Tropical Ecology, 43*, 39–47.

Sahebjalal, E., & Dashtekian, K. (2013). Analysis of land use land covers changes using normalized difference vegetation index (NDVI) differencing and classification methods. *African Journal of Agriculture Research, 8*, 4614–4622.

Seddon, A. W. R., Macias-Fauria, M., Long, P. R., Benz, D., & Willis, K. J. (2016). Sensitivity of global terrestrial ecosystems to climate variability. *Nature, 531*(7593), 229–232.

Shamir, E., & Georgakakos, K. P. (2014). MODIS land surface temperature as an index of surface air temperature for operational snowpack estimation. *Remote Sensing of Environment, 152*, 83–98.

Srivastava, P. K., Majumdar, T. J., & Bhattacharya, A. K. (2009). Surface temperature estimation in Singhbhum Shear Zone of India using Landsat-7 ETM-f thermal infrared data. *Advances in Space Research, 4*, 1563–1574.

Stewart, I. D. (2000). Influence of meteorological conditions on the intensity and form of the urban heat island effect in Regina. *Canadian Geographer, 44*, 271–285.

Stocker, T. F., Qin, D., Plattner, G. K., Tignor, M., Allen, S. K., Boschung, J., Nauels, A., Xia, Y., Bex, V., & Midgley, P. M. (2013). Summary for policymakers. In climate change 2013: the physical science basis. Contribution of Working Group I to the Fifth Assessment Report of the Intergovernmental Panel on Climate Change. Cambridge: Cambridge University Press.

Sun, Z. D., Chang, N. B., & Opp, C. (2010). Using SPOT-VGT NDVI as a successive ecological indicator for understanding the environmental implications in the Tarim River basin, China. *Journal of Applied Remote Sensing, 4*, 844–862.

Voogt, J., & Oke, T. (2003). Thermal remote sensing of urban climates. *Remote Sensing of Environment, 86*, 370–384.

Wanders, N., Bierkens, M. F. P., de Jong, S. M., & de RooA, K. D. (2014). The benefits of using remotely sensed soil moisture in parameter identification of large-scale hydrological models. *Water Resources Research, 50*, 6874–6891.

Waylen, P., Southworth, J., Gibbes, C., & Tsai, H. (2014). Time series analysis of land cover change: developing statistical tools to determine significance of land cover changes in persistence analyses. *Remote Sensing, 6*, 4473–4497.

Weng, Q. (2009). Thermal infrared remote sensing for urban climate and environmental studies: methods, applications, and trends. *ISPRS Journal of Photogrammetry and Remote Sensing, 2009*(64), 335–344.

Weng, Q., Lu, D., & Schubring, J. (2004). Estimation of land surface temperature-vegetation abundance relationship for urban heat island studies. *Remote Sensing of Environment, 89*, 467–483.

Wilson, J. S., Clay, M., Martin, E., Stuckey, D., & Vedder-Risch, K. (2003). Evaluating environmental influences of zoning in urban ecosystems with remote sensing. *Remote Sensing of Environment, 86*, 303–321.

Winckler, J., Reick, C. H., & Pongratz, J. (2017). Why does the locally induced temperature response to land cover change differ across scenarios? *Geophysical Research Letters, 44*, 3833–3840.

Xu, H. Q. (2006). Modification of normalised difference water index (NDWI) to enhance open water features in remotely sensed imagery. *International Journal of Remote Sensing, 27*, 3025–3033.

Xu, H. Q., Ding, F., & Wen, X. L. (2009). Urban expansion and heat island dynamics in the Quanzhou region, China. *IEEE Journal of Selected Topics in Applied Earth Observations and Remote Sensing, 2*, 1939–1404.

Xu, H. Q., Huang, S. L., & Zhang, T. J. (2013). Built-up land mapping capabilities of the ASTER and Landsat ETM+ sensors in coastal areas of southeastern China. *Advances in Space Research, 52*, 1437–1449.

Yuan, F., & Bauer, M. E. (2007). Comparison of impervious surface area and normalized difference vegetation index as indicators of surface urban heat island effects in Landsat imagery. *Remote Sensing of Environment, 106*, 375–386.

Zawadzki, J., Cieszewski, C. J., Zasada, M., & Lowe, R. C. (2005). Applying geostatistics for investigations of forest ecosystems using remote sensing imagery. *Silva Fennica, 39*, 599–618.

Zha, Y., Gao, J., & Ni, S. (2003). Use of normalized difference built-up index in automatically mapping urban areas from TM imagery. *International Journal of Remote Sensing, 24*, 583–594.

Zhou, D., Zhang, L., Li, D., Huang, D., & Zhu, C. (2016). Climate-vegetation control on the diurnal and seasonal variations of surface urban heat islands in China. *Environmental Research Letters, 11*, 074009.

Zhuo, L., Dai, Q., & Han, D. (2015). Evaluation of SMOS soil moisture retrievals over the central United States for hydrometeorological application. *Physics and Chemistry of the Earth, Parts A/B/C, 83-84*, 146–155.